nature neuroscience

Excitatory transmission at thalamo-striatal synapses mediates susceptibility to social stress

Daniel J Christoffel[1,2,6], Sam A Golden[1,6], Jessica J Walsh[1,3], Kevin G Guise[1], Mitra Heshmati[1], Allyson K Friedman[3], Aditi Dey[1], Milo Smith[1], Nicole Rebusi[1], Madeline Pfau[1], Jessica L Ables[4], Hossein Aleyasin[1], Lena A Khibnik[1], Georgia E Hodes[1], Gabriel A Ben-Dor[2], Karl Deisseroth[2,5], Matthew L Shapiro[1], Robert C Malenka[2], Ines Ibanez-Tallon[4], Ming-Hu Han[1,3] & Scott J Russo[1]

Postsynaptic remodeling of glutamatergic synapses on ventral striatum (vSTR) medium spiny neurons (MSNs) is critical for shaping stress responses. However, it is unclear which presynaptic inputs are involved. Susceptible mice exhibited increased synaptic strength at intralaminar thalamus (ILT), but not prefrontal cortex (PFC), inputs to vSTR MSNs following chronic social stress. Modulation of ILT-vSTR versus PFC-vSTR neuronal activity differentially regulated dendritic spine plasticity and social avoidance.

The vSTR is an important initiator of reward-related behaviors[1,2] that undergoes synaptic remodeling following chronic social defeat stress (CSDS), leading to depression-like behavior[3,4]. Multiple glutamatergic inputs to vSTR regulate reward-related behaviors[5,6] and it is unclear which mediate the effects of chronic stress. The ILT and PFC send prominent projections to striatum and may serve opposing roles in stress and reward-related behaviors[7–11]. We found that excitatory transmission at ILT-vSTR synapses controlled susceptibility to social stress, whereas modulation of PFC-vSTR projections had distinct effects, possibly mediated by efferents outside of the vSTR.

We employed a dual virus approach, where retrogradely transported AAV2/5-Cre was injected into vSTR and Cre-inducible AAV expressing EYFP into the ILT to examine the axonal arborization patterns of the ILT- and PFC-vSTR projections (**Fig. 1**). Notably, the strength of innervation of each projection appeared to vary widely throughout discrete striatal subregions (**Fig. 1b**,**f**). To examine stress-induced synaptic adaptations, we immuno-stained vSTR for vesicular glutamate transporters 1 and 2 (VGLUT1 and VGLUT2), which are enriched in cortical and thalamic inputs, respectively[12]. Susceptible mice are socially avoidant[13–15] and exhibited an increase in VGLUT2, but not VGLUT1 (**Supplementary Fig. 1**). To measure the effects of CSDS on synaptic plasticity at ILT- or PFC-vSTR synapses, we expressed AAV-channelrhodopsin (pAAV-DJ-Ef1a-ChR2 (H134R)-EYFP; referred to as ChR2) in ILT or PFC and prepared acute brain slices of the vSTR 48 h after CSDS. We measured the ratio of optically evoked α-AMPA receptor (AMPAR)-mediated to NMDA receptor (NMDAR)-mediated currents (AMPAR/NMDAR ratio). The AMPAR/NMDAR ratio was increased only at ILT inputs to MSNs of susceptible mice (**Fig. 1c**,**d**), with no change at PFC inputs (**Fig. 1g**,**h**) or with non-selective electrical activation (**Supplementary Fig. 2**).

To assess whether ILT-vSTR activity mediates CSDS-induced social avoidance and spine plasticity in the vSTR[4], we used the dual virus

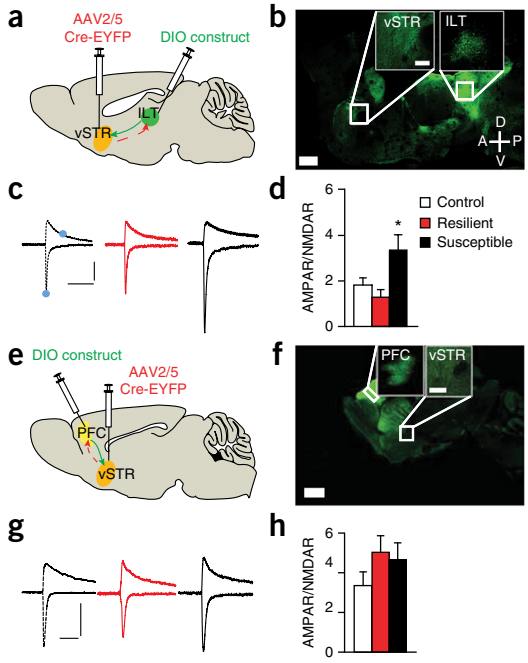

Figure 1 Stress-induced circuit-specific synaptic adaptations. (**a**,**e**) Two virus strategy for targeting of ILT-vSTR (**a**) and PFC-vSTR (**e**) projections. (**b**,**f**) Confocal image of a single sagittal mouse slice of EYFP-expressing ILT-vSTR (**b**) and PFC-vSTR (**f**) projection neurons (patterns examined in three mice per projection; scale bars represent 1 mm and 200 µm (inset). (**c**,**d**,**g**,**h**) Example traces (**c**,**g**) and quantification (**d**,**h**) of oEPSCs at −70 mV and +40 mV for ILT-vSTR (control, resilient, susceptible, $n = 11$, 8, 9 cells, 4, 3, 3 mice, one-way ANOVA, $^*P = 0.014$, $F_{2,25} = 5.075$), and PFC-vSTR synapses (control, resilient, susceptible, $n = 8$, 8, 7 cells, 3, 3, 3 mice, one-way ANOVA, $P = 0.524$, $F_{2,20} = 0.268$). Solid blue dots indicate the current amplitude used to calculate the AMPAR/NMDAR ratio. Scale bars represent 100 pA and 100 ms. All error bars represent s.e.m.

[1]Fishberg Department of Neuroscience, Friedman Brain Institute Graduate School of Biomedical Sciences, Icahn School of Medicine at Mount Sinai, New York, New York, USA. [2]Nancy Pritzker Laboratory, Department of Psychiatry and Behavioral Sciences, Stanford University, Stanford, California, USA. [3]Department of Pharmacology and Systems Therapeutics, Graduate School of Biomedical Sciences, Icahn School of Medicine at Mount Sinai, New York, New York, USA. [4]Laboratory of Molecular Genetics, Howard Hughes Medical Institute, Rockefeller University, New York, New York, USA. [5]Department of Bioengineering, Stanford University, Stanford, California, USA. [6]These authors contributed equally to this work. Correspondence should be addressed to S.J.R. (scott.russo@mssm.edu).

Received 23 March; accepted 5 May; published online 1 June 2015; doi:10.1038/nn.4034

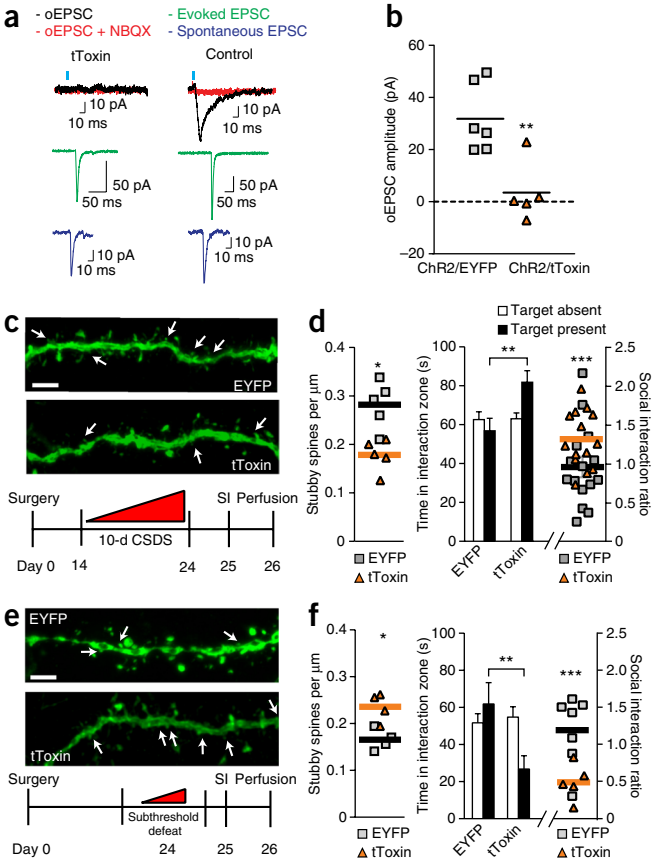

Figure 2 tToxin-mediated inhibition of ILT-vSTR and PFC-vSTR projections regulates stress-induced behavioral and synaptic plasticity. (**a**) Representative traces of EPSCs from vSTR MSNs; left, ChR2 + tToxin; right, ChR2 + EYFP control. Each trace is 20 responses from a cell averaged. (**b**) Average oEPSC amplitude (EYFP, tToxin, $n = 5$, 6 cells, 2, 2 mice, unpaired t test, $^{**}P = 0.004$, $t = 3.796$ df = 9). (**c**) Top, three-dimensional reconstructions of MSN dendrites (white arrows indicate stubby spines, scale bar represents 5 µm). Bottom, experimental timeline for ILT-vSTR circuit. (**d**) Left, quantification of stubby spine densities ($n = 5$ mice per group, unpaired t test, $^{*}P = 0.003$, $t = 4.017$, df = 8). Right, quantification of time spent in the interaction zone and social interaction ratio (EYFP, tToxin, $n = 15$, 14 mice, two-way ANOVA (time spent), $^{**}P = 0.019$, $F_{1,54} = 5.809$ (interaction), unpaired t test (social interaction (SI) ratio), $^{***}P = 0.04$, $t = 2.143$, df = 27). (**e**) Top, three-dimensional reconstructions of MSN dendrites (white arrows indicate stubby spines, scale bar represents 5 µm). Bottom, experimental timeline for PFC-vSTR circuit. (**f**) Left, quantification of stubby spine densities ($n = 4$ mice per group, unpaired t test, $^{*}P = 0.014$, $t = 3.421$, df = 6). Right, quantification of time spent in the interaction zone and social interaction ratio (EYFP, tToxin, $n = 7$, 5 mice, two-way ANOVA (time spent), $^{**}P = 0.034$, $F_{1,20} = 5.170$ (interaction), unpaired t test (SI ratio), $^{***}P = 0.013$, $t = 3.013$, df = 10). All error bars represent s.e.m.

approach described above (**Fig. 1a**,**e**) to express AAV2-ω-agatoxin and AAV2-ω-conotoxin, 'tToxins', in ILT-vSTR pathway. tToxins block calcium influx at the presynaptic voltage-gated Ca^{2+} channels Cav2.1 and Cav 2.2 (ref. 16). We found that tToxins expression blocked optically evoked excitatory postsynaptic currents (oEPSCs) in vSTR MSNs (**Fig. 2a**,**b**). Electrically stimulated EPSCs and spontaneous EPSCs were similar in both groups (**Fig. 2a**), whereas oEPSCs were blocked by the AMPAR antagonist NBQX (**Fig. 2a**). Confocal analysis of ILT terminal fields in vSTR showed nearly 100% colocalization between the tToxin viruses (**Supplementary Fig. 3a**), with no evidence of toxicity produced by expression of tToxins, assessed by a lack of activated caspase-3 (Cas3) (**Supplementary Fig. 3b**).

Following expression of AAV-tToxins, we exposed mice to CSDS, measured social interaction and collected tissue for spine analysis 24 h later. tToxin-mediated inhibition of ILT-vSTR neurons reduced MSN stubby spine density and social avoidance (**Fig. 2c**,**d**). Spine density correlated with social interaction ratio and no group exhibited locomotor deficits (**Supplementary Fig. 4**). Next, following expression of tToxins in PFC-vSTR MSNs, we exposed mice to subthreshold defeat and found increased vSTR stubby spine density and social avoidance, mimicking a susceptible phenotype (**Fig. 2e**,**f**). However, spine density did not correlate with social avoidance (**Supplementary Fig. 5**) and may be a homeostatic adaptation unrelated to the changes at ILT-vSTR synapses and social avoidance behavior described above. As expected, there were no effects on locomotion (**Supplementary Fig. 5**) and no changes in other spine types in either experiment (**Supplementary Fig. 6**)[4].

To achieve greater pathway specificity, we used AAV-ELFa-DIO-eNpHR3.0-EYFP-WPRE-pA (referred to as NpHR) coupled with injection of AAV2/5-Cre into the vSTR and implanted a fiber optic into vSTR to silence specific presynaptic terminal fields. We used *in vivo* optical stimulation of ILT-vSTR neuron somas coupled to multi-unit recording to determine optimal parameters for inhibiting firing (**Fig. 3a**). We employed a terminal inhibition strategy that reduces neuronal firing rate in the projection region and alters behavior[17]. Inhibition of ILT-vSTR during social interaction reversed stress-induced social avoidance similar to tToxins without affecting locomotion (**Fig. 3b** and **Supplementary Fig. 7a**,**b**). Rapid inhibition of PFC terminals had no effect on social interaction (**Fig. 3c** and **Supplementary Fig. 7c**,**d**), suggesting that social avoidance is either regulated by PFC efferents to regions outside of the vSTR that are silenced by tToxin, but not NpHR, or that sustained inhibition of PFC-vSTR inputs is required.

To determine whether circuit activation is sufficient to promote social avoidance, we expressed AAV2/5-Cre in the vSTR and Cre-inducible AAV-ChR2 in the PFC or ILT and performed a subthreshold defeat. ChR2 stimulation parameters were validated in acute slices from ILT or PFC (**Supplementary Fig. 8a**,**b**) and *in vivo* by optical stimulation of ILT-vSTR projecting neurons coupled to multi-unit recording (**Fig. 3d**). We were able to reliably induce firing of ILT neurons without altering spike waveforms. Stimulation of ILT-vSTR somas reduced social interaction, whereas stimulation of PFC-vSTR had no effect (**Fig. 3e**,**f** and **Supplementary Fig. 8c**,**d**). Locomotion was not affected in any group (**Supplementary Fig. 8e**,**f**). We performed ChR2-mediated ILT terminal stimulation directly in the vSTR and found that this also reduced social interaction without affecting locomotion (**Supplementary Fig. 9**). Although we cannot rule out back-propagating action potentials, ChR2 terminal stimulation produced opposite behavioral effects compared with NpHR terminal stimulation. Consistent with previous reports, high-frequency (100 Hz) stimulation of PFC terminals in vSTR had an anti-depressant effect (**Supplementary Fig. 10**)[7,18], although we have to caution that these parameters are outside of the kinetic range of ChR2 and further studies are needed to interpret these results.

Our data provides evidence that thalamic inputs to vSTR have a prominent role in regulating aversive responses to stress, in contrast with reports that other glutamatergic inputs to the vSTR, including the PFC and amygdala, promote reward[5,6]. Increased glutamatergic transmission at the ILT-vSTR circuit mediated stress-induced vSTR postsynaptic plasticity, as well as susceptibility to social stress. We observed no changes in the strength of PFC-vSTR synapses and

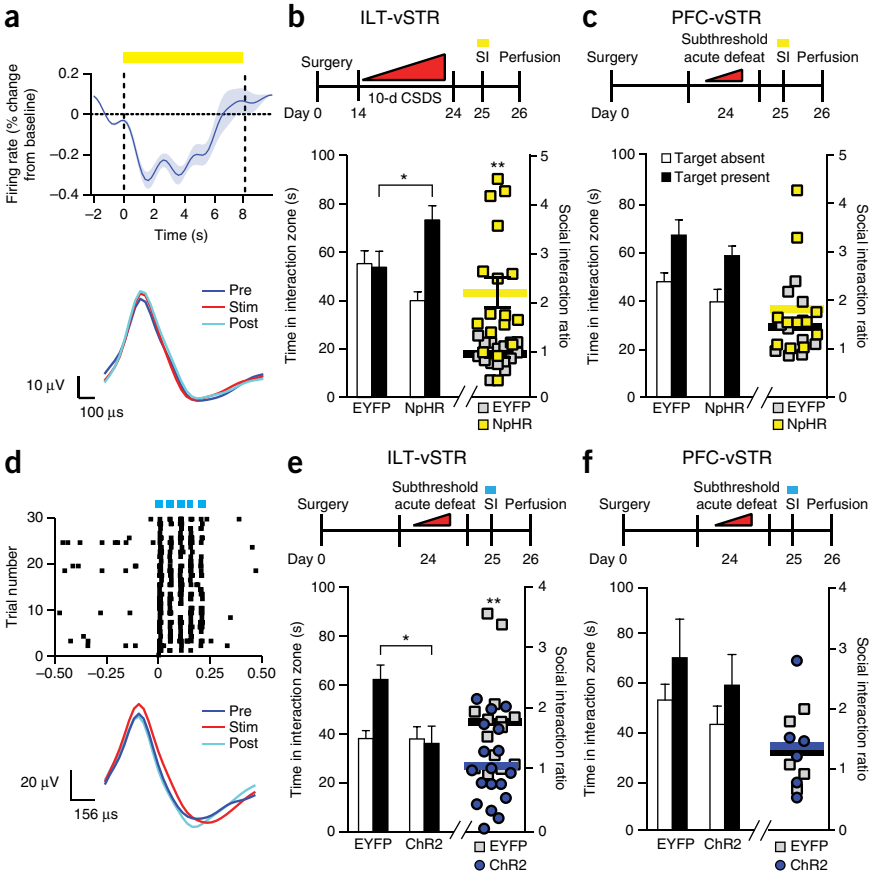

Figure 3 Rapid circuit-specific optogenetic regulation of social avoidance. (**a**) *In vivo* NpHR validation. Top, averaged firing rate (% change from baseline; s.e.m. in light blue) during yellow light On/Off epochs ($n = 56$ trials, 4 cells, 1 mouse). Bottom, averaged representative waveforms. (**b**) Experimental timeline for ILT-vSTR circuit inhibition with NpHR (top) and quantification of time spent in the interaction zone and social interaction ratio (EYFP/NpHR, $n = 16/17$ mice, two-way ANOVA (time spent), $^{*}P = 0.002$, $F(1,62) = 10.15$ (interaction); unpaired t test (SI ratio), $^{**}P = 0.0005$, $t = 3.894$, df = 31). (**c**) Experimental timeline for PFC-vSTR circuit inhibition with NpHR (top) and quantification of time spent in the interaction zone and social interaction ratio ($n = 11$ mice per group, two-way ANOVA (time spent), $P = 0.989$, $F(1, 40) = 0.0001775$ (interaction); unpaired t test (SI ratio), $P = 0.360$, $t = 1.050$, df = 20). (**d**) *In vivo* ChR2 validation. Top, raster plots of spike events per trial; blue light evoked time-locked spikes in 30 trials (1 mouse). Bottom, representative spike waveforms. (**e**) Experimental timeline of ILT-vSTR circuit (top) and quantification of time spent in the interaction zone and social interaction (EYFP/NpHR, $n = 14/18$ mice, two-way ANOVA interaction (time spent), $^{*}P = 0.027$, $F(1,60) = 5.087$; unpaired t test (SI ratio), $^{**}P = 0.008$, $t = 2.802$, df = 30). (**f**) Schematic and experimental timeline of PFC-vSTR circuit (top) and quantification of time spent in the interaction zone and social interaction ratio (EYFP/NpHR, $n = 5/6$ mice, two-way ANOVA (time spent), $P = 0.953$, $F(1, 18) = 0.003529$ (interaction); unpaired t test (SI ratio), $P = 0.831$, $t = 0.2191$, df = 9). All error bars represent s.e.m.

only chronic inhibition of PFC affected social avoidance and vSTR spine density. Despite the vSTR spine changes induced by chronic PFC inhibition with tToxins, spine density changes did not correlate with social avoidance behavior and neither rapid terminal specific activation nor inhibition of PFC-vSTR synapses affected social avoidance, suggesting that tToxin-mediated inhibition of PFC neurons may be acting via other brain circuits and downstream mechanisms. Lastly, although our results suggest that two distinct glutamatergic inputs to the vSTR have divergent roles in the behavioral response to stress, it is becoming increasingly apparent that distinct NAc inputs have integral, but highly specific, roles in the regulation of stress responses[19,20]. Taken toghether, these results highlight the complexities of brain reward circuits and the need for future research to more completely define the synaptic and behavioral adaptations induced in other glutamatergic microcircuits in response to a range of stressful experience.

METHODS

Methods and any associated references are available in the online version of the paper.

Note: Any Supplementary Information and Source Data files are available in the online version of the paper.

ACKNOWLEDGMENTS

This research was supported by US National Institute of Mental Health grants R 01 MH090264 (S.J.R.), R01 MH092306 (M.-H.H.), P50 MH096890 (S.J.R. and M.-H.H.), T32 GM089626 (D.J.C.), T32 MH087004 (M.P. and M.H.), F31 MH105217 (M.P.), F32 MH096464 (A.K.F.), P01 DA008227 (R.C.M.) and F30 MH100835 (M.H.).

AUTHOR CONTRIBUTIONS

D.J.C., S.A.G. and S.J.R. designed the studies, interpreted the results and wrote the paper. D.J.C., S.A.G., J.J.W., M.H., A.K.F., H.A., L.A.K., N.R., M.P., G.A.B.-D. and G.E.H. performed stereotactic injections, optogenetic experiments and electrophysiology. K.G.G., S.A.G. and M.L.S. performed *in vivo* ChR2 validation. D.J.C., A.D., J.L.A. and M.S. performed immunohistochemistry. J.L.A. and I.I.-T. generated viruses. K.D., J.J.W., A.K.F., R.C.M. and M.-H.H. provided optogenetics and electrophysiology training. All of the authors edited the paper.

COMPETING FINANCIAL INTERESTS

The authors declare no competing financial interests.

1. Christoffel, D.J., Golden, S.A. & Russo, S.J. *Rev. Neurosci.* **22**, 535–549 (2011).
2. Russo, S.J. & Nestler, E.J. *Nat. Rev. Neurosci.* **14**, 609–625 (2013).
3. Golden, S.A. *et al. Nat. Med.* **19**, 337–344 (2013).
4. Christoffel, D.J. *et al. J. Neurosci.* **31**, 314–321 (2011).
5. Britt, J.P. *et al. Neuron* **76**, 790–803 (2012).
6. Stuber, G.D. *et al. Nature* **475**, 377–380 (2011).
7. Covington, H.E. III *et al. J. Neurosci.* **30**, 16082–16090 (2010).
8. Bubser, M. & Deutch, A.Y. *Synapse* **32**, 13–22 (1999).
9. Browning, J.R., Jansen, H.T. & Sorg, B.A. *Drug Alcohol Depend.* **134**, 387–390 (2014).
10. Chen, B.T. *et al. Nature* **496**, 359–362 (2013).
11. Penzo, M.A. *et al. Nature* **519**, 455–459 (2015).
12. Fremeau, R.T. Jr. *et al. Neuron* **31**, 247–260 (2001).
13. Berton, O. *et al. Science* **311**, 864–868 (2006).
14. Krishnan, V. *et al. Cell* **131**, 391–404 (2007).
15. Golden, S.A., Covington, H.E. III, Berton, O. & Russo, S.J. *Nat. Protoc.* **6**, 1183–1191 (2011).
16. Auer, S. *et al. Nat. Methods* **7**, 229–236 (2010).
17. Kim, S.-Y.Y. *et al. Nature* **496**, 219–223 (2013).
18. Vialou, V. *et al. J. Neurosci.* **34**, 3878–3887 (2014).
19. Tye, K.M. *et al. Nature* **493**, 537–541 (2013).
20. Chaudhury, D. *et al. Nature* **493**, 532–536 (2013).

ONLINE METHODS

Animals. 6–10-week-old male C57BL/6J mice (Charles River Laboratories) were used for all experiments. For social defeat studies, 4-month-old retired CD-1 breeders (Jackson Laboratories) were used as aggressors. 1 week before the start of all experiments, mice were group housed and maintained on a 12-h light/dark cycle with *ad libitum* access to food and water. All animals were randomly assigned to each experimental group. Behavioral assessments and tissue collection were performed during the animals' light phase (7:00–19:00 h). Mouse procedures were performed in accordance with the Institutional Animal Care and Use Committee guidelines of the Icahn Sinai School of Medicine at Mount Sinai.

Stereotaxic surgery and viral gene transfer. *Dual virus approach.* An injection of a adeno-associated virus (AAV) expressing Cre recombinase, of a recombinant serotype known to retrograde[21], (AAV2/5-Cre) into the vSTR and a Cre-dependent AAV containing the vector of interest into the ILT or the PFC was used to isolate projection neurons in all studies.

Injection protocol and coordinates. C57BL/6J mice were anesthetized with a mixture of ketamine (100 mg per kg of body weight) and xylazine (10 mg per kg) and positioned in a small-animal stereotaxic instrument (David Kopf Instruments), and the skull surface was exposed. 33 gauge syringe needles (Hamilton) were used to bilaterally infuse 0.5 µl of rAAV2/5CMV.Cre-GFP, ($1.5 \times 10^{11-13}$ infectious units per ml, UPenn Viral Vector Core) into the vSTR (bregma coordinates: anteroposterior, 1.5 mm; mediolateral, 1.6 mm; dorsoventral, 4.4 mm; angle 10°) at a rate of 0.1 µl min^{-1}. For optogenetic studies, either pAAV-Ef1a-DIO-EYFP (DIO-EYFP) or pAAV-Ef1a-DIO-ChR2 (H134R)-EYFP (DIO-ChR2) were injected into the ILT (bregma coordinates: anteroposterior, −2.2 mm; mediolateral, 1.5 mm; dorsoventral, −4.1 mm; angle 10°) or the PFC (bregma coordinates: anteroposterior, 1.9 mm; mediolateral, 0.8 mm; dorsoventral, −2.2 mm; angle 10). For all optogenetic experiments, animals were implanted with handmade optical fibers of 200 µm in diameter 0.22 NA silicon core (ThorLabs)[22]. 2 weeks following viral injection using the same coordinates for each region. For studies using tToxins to inhibit neurotransmission, either DIO-EYFP or Cre inducible membrane-tethered ω-agatoxin and ω-conotoxin, fused with mCherry and EYFP, respectively (pAAV2/8-CMV-DIO-Agatoxin-mCherry and pAAV2/8-CMV-DIO-conotoxin-EYFP), referred to as tToxins were injected at the above coordinates for the ILT or PFC.

Blue light stimulation. Animals received either stimulation of the PFC- or ILT-vSTR pathway for two 2.5-min trials during the social interaction test. Light was off in between trials. Blue light was delivered at a frequency of 20 Hz (20-ms pulse width) and five pulses were delivered in a burst with a burst period of 1 s using a 100-mW DPSS 498-nm laser (OEM Laser). Intensity of light delivered to ferrule was ~10 mW.

Electrophysiology. *In vitro.* Whole-cell recordings were obtained from ILT, PFC, and vSTR neurons in acute brain slices from mice that had been stereotaxically injected with DIO-ChR2 into the ILT or PFC and rAVV2/5-Cre into the vSTR for validation of *in vivo* stimulation parameters or ChR2 only into the ILT or PFC for synaptic physiology studies. To minimize stress and to obtain healthy slices, mice were anaesthetized and perfused immediately for 40-60 s with ice-cold artificial cerebrospinal fluid (aCSF), which contained in mM: 126 NaCl, 1.6 KCl, 1.2 NaH_2PO_4, 11 D-glucose, 18 $NaHCO_3$, 2.5 $CaCl_2$ and 1.2 $MgCl_2$ (oxygenated with 95% O_2 and 5% CO_2, pH 7.4, 295–305 mOsm). Acute brain slices were cut using a microslicer (DTK-1000, Ted Pella) in cold sucrose aCSF which contained in mM: 254 mM sucrose, 23 KCl, 1.25 NaH_2PO_4, 10 D-glucose, 24 $NaHCO_3$, 2 $CaCl_2$ and 2 $MgCl_2$ saturated by 95% O_2 and 5% CO_2. Slices were maintained in holding chambers with aCSF for 1 h at 32 °C. Patch pipettes (3–5 mΩ) for whole-cell current-clamp recordings were filled with internal solution containing the following (mM): 115 potassium gluconate, 20 KCl, 1.5 $MgCl_2$, 10 phosphocreatine, 10 HEPES, 2 magnesium ATP and 0.5 GTP (pH 7.2, 285 mOsm). Patch pipettes (3–5 mΩ) for voltage-clamp recordings were filled with internal solution containing the following (mM): 117 cesium methanesulfonate, 2.8 NaCl, 0.4 EGTA, 5 tetraethylammonium chloride, 20 HEPES, 24 magnesium ATP and 0.4 GTP (pH 7.2, 285 mOsm). Whole-cell recordings were carried out using aCSF at 32 °C (flow rate = 2.5 ml min^{-1}). For validation of *in vivo* optogenetic stimulation protocols, resting membrane potential and action potentials were recorded in current-clamp mode using the Multiclamp 700B amplifier and data acquisition was done in pClamp 10 (Molecular Devices). Trains (20-Hz, 20-ms pulse width, 5 pulse per s) of blue light were generated by a wave-form generator (Agilent Technologies) and delivered to neurons expressing ChR2 through a 200-µm diameter optic fiber attached to a 473-nm laser. The fiber was placed directly above the slice and stimulated the entire area of interest.

Postsynaptic recordings from MSNs were made in areas of high ChR2 terminal infectivity while activating ChR2 with 473-nm blue light. Whole-cell voltage-clamp recordings were carried out using aCSF with the addition of 100 µm picrotoxin to block $GABA_A$ receptor currents at 32 °C (flow rate = 2.5 ml min^{-1}). Recordings from MSNs were obtained under visual control using a 40× objective. The vSTR was identified by the presence of the anterior commissure. Series resistance (10–25 MΩ) was monitored with a 5-mV hyperpolarizing pulse (10 ms) given during every epoch, and only recordings that remained stable over the period of data collection were used. For circuit specific AMPAR/NMDAR experiments, during each 1.5-s epoch, a 1-ms blue light pulse and a 0.2-ms electrical pulse was delivered, separated by 500 ms. The blue light was delivered by an LED (ThorLabs) directed through the objective with an intensity of ~10 mW. Electrical stimulation was delivered with a bipolar nichrome wire electrode placed at the border between the NAc and the cortex dorsal to the anterior commissure. Each 1.5-s epoch was separated by 10 s. For tToxin validation experiments, during a 1-s epoch, 5-ms blue light pulse and a 0.2-ms electrical pulse was delivered, separated by 500 ms. Each 1-s epoch was separated by 10 s. Recordings were performed using a Multiclamp 700B (Molecular Devices), filtered at 3 kHz and digitized at 10 kHz. Data acquisition and analysis were performed using AxoGraph X. Experimenter was blind to experimental condition during recordings and analysis.

In vivo optrode construction. An optrode was constructed by gluing four tetrodes to an optical fiber. Four tetrodes spun of 12.7-µm diameter nichrome wire (California Fine Wire) were glued to a 200-µm diameter optical fiber (Thorlabs) and cut so that they extended between 250 and 750 µm beyond the end of the fiber. The tetrodes were pinned into an electrode interface board (EIB; Neuralynx) and the tips were plated by passing 0.2 µA current pulses through the individual wires and a gold solution until the impedance reached 150–200 kOhm. The optrode was mounted on a stereotax arm (Kopf) so that it could be lowered into the brain during surgery.

Surgery. Animals were anesthetized and placed in a stereotax (Kopf). The scalp was resected and the head position was adjusted so that bregma and lambda were level. Burr holes were drilled for the vSTR (see previous coordinates). Two small holes were drilled anterior and posterior to the recording site to serve as sites for ground screws. The ground screws were constructed by soldering stainless steel self-tapping screws to 3 mil stainless steel wire which were pinned into the EIB. Screws were inserted far enough to come in contact with dura.

In vivo recording. Recordings were carried out using a Digital Lynx 16SX recording system and Cheetah data acquisition software (Neuralynx). Signals from the tetrodes were bandpass filtered between 600 and 9,000 Hz and digitized at 32 kHz. Spike detection was performed in real time using a thresholding procedure: when the filtered signal reached threshold amplitude on any wire, a sweep including 8 data points before the crossing and 24 points after (32 points, or 1 ms) were saved as a putative spike event. Spike sorting and noise filtering was performed offline.

The recording stimulation protocol was the same as during the experiment proper: for ChR2, a 5 pulse burst (20 Hz with a 40% duty cycle) was delivered once every second. A recording trial was defined as the epoch encompassing the 500 ms leading up to the burst onset to 500 ms after. Markers were set in the recording record for the onset of each pulse for both baseline and stimulation epochs despite the laser being turned off during the baseline epochs. For the NpHR experiment, the laser was pulsed on and off every 10 s with an 8-s duty cycle (8 s on, 2 s off) for 2 min. A recording trial was defined as the 2 s leading up to the laser onset, up to 2 s following its offset.

For the ChR2 experiments, the laser intensity was adjusted so that ~10 mV was emitted from the tip of the optrode, and then it was lowered until the tetrode tips reached the dorsal extent of the ILT. Once the tissue and recordings

doi:10.1038/nn.4034

stabilized, the optrode was advanced until spikes were observed on at least one of the tetrodes. Recording started if the spike amplitude and rate appeared stable over the course of several minutes. Thirty trials of baseline recordings were then acquired, immediately followed by 30 trials of stimulation recordings, and 30 trials of post-stimulus baseline. The optrode was then stepped forward and the same procedure was repeated until the ventral extent of the ILT was reached. For the NpHR experiment, a 2 min baseline without stimulation was acquired, followed by 2 min of the stimulation protocol described above, and a 2-min post-stimulation baseline.

In vivo recording analysis. Data were analyzed using custom scripts written in Matlab (MathWorks). A first round of preliminary spike sorting was carried out using spike waveforms as parameters in KlustaKwik. The output from KlustaKwik was then imported into Matlab and clusters were manually edited using custom spike sorting software. Clearly separated clusters of spikes were assigned to functional units and entered into further analysis; noise spikes (for example, from spurious threshold crossings) were discarded. Peri-stimulus time histograms for each unit were generated by binning spike counts in non-overlapping 2 ms bins and summing over trials for the baseline and stimulation epochs. For the NpHR experiment, data were binned in 200 ms epochs and the resulting trial-wise rate functions were smoothed with a Gaussian window of 1 s s.d. and values adjusted to % of baseline before averaging.

CSDS. Chronic social defeat stress was performed as described previously[8–10]. Experimental C57BL/6J mice were exposed to a novel CD1 aggressor for 10 min daily over 10 consecutive days. CD1 mice 4–5 months old were selected for aggressive behavior based on criteria previously described[8]. After 10 min of physical contact, experimental mice were removed and placed on the opposite side of the aggressor's home cage behind a "protective" partition that was perforated with holes to allow for sensory contact during the following 24 h. Control mice were housed two animals per cage under the same conditions as their experimental counterparts but without the presence of an aggressive CD1 mouse. Experimental mice were relocated to a new cage each day immediately before the social defeat. 24 h after the final social defeat, all mice were housed individually. To measure increased susceptibility to stress we adapted a subthreshold defeat as previously described[9]. For optogenetic studies, C57BL/6J mice were exposed to a novel CD1 aggressor for 5 min, followed by 10 min on the opposite side of the aggressor's home cage behind a 'protective' partition, and 5-min rest in the home cage. Exposure to the CD1 aggressor occurred three times with 5-min intervals between each exposure. For tToxin studies, C57BL/6J mice were exposed to a novel CD1 aggressor for 5 min, followed by 5-min rest in the home cage. Exposure to the CD1 aggressor occurred 3 times with 5 min intervals between each exposure. 24 h later mice were assessed using the social interaction test.

Social interaction. Social interaction was performed as previously described[8,10]. Mice were placed into a novel arena with a small animal cage at one end. Their movement was monitored for 2.5 min in the absence of an aggressive CD1 mouse (used to determine baseline exploratory behavior), followed by 2.5 min in the presence of the caged aggressor. We measure the distance traveled (in centimeters), duration spent in the interaction zone and corner zones (in seconds) using Ethovision 3.0 software (Noldus Information Technology). We calculated social interaction as a ratio of the time spent in the interaction zone with an aggressive mouse present over the time spent with the aggressive mouse absent. All mice with a ratio above 1 were classified as resilient and all mice with a ratio below 1 were classified as susceptible.

Perfusion and tissue processing. All mice were given a fatal dose of 15% chloral hydrate and transcardially perfused with cold 1% paraformaldehyde in phosphate-buffered saline (PBS; pH 7.4), followed by fixation with cold 4% paraformaldehyde in PBS. Brains were dissected and postfixed for 18 h in the same fixative. Coronal sections were prepared on a vibratome (Leica) at 50 µm to assess viral placement or immunohistochemistry and 150 µm for spine analysis.

Immunohistochemistry. Coronal sections (50 µm thick) were used for all immunofluorescence experiments. Sections were incubated in blocking solution (3% normal donkey serum, 0.3% Triton X-100 in PBS) for 1 h. Sections were then incubated in primary antibody overnight at 4 °C (chicken anti-GFP (Aves) 1:3,000; rabbit anti-RFP (Abcam #ab62341) 1:500; guinea pig anti-VGLUT1 (Millipore #ab5905) 1:2,000; guinea pig anti-VGLUT2 (Millipore, #ab2251) 1:1,000). Sections were washed in PBS for 30 min, incubated in secondary antibody for 2 h (donkey anti-chicken Cy2 1:200; donkey anti-rabbit Cy3 1:200; donkey anti-guinea pig Cy3 1:200 (Jackson ImmunoResearch)), then washed in PBS for 30 min, mounted and air-dried overnight. Slides were coverslipped with Vectashield (Jackson ImmunoResearch).

For tToxin representative images, antibodies directed against the attached fluorophore, for ω-agatoxin against mCherry and for ω-conotoxin against EYFP, were used to enhance the detectable fluorescence. Activated caspase staining was performed to rule out toxicity from tToxin infection. Sections were mounted on SuperFrost Plus slide for antigen retrieval (10 mM citric acid, pH 6, 95 °C, 15 min). After antigen retrieval, slides were immersed in room temperature 1× TBS to cool for 5 min. Sections were circled with a PAP pen and slides were placed in a humidified chamber. All incubations were performed on the bench top at room temperature. Sections were blocked in 3% normal donkey serum and 0.3% Triton X-100 in 1× TBS for 15 min. Sections were incubated in the following primaries diluted in blocking solution overnight: Chicken anti-GFP (1:500, Aves Labs, #GFP-1020), rabbit anti-RFP (1:1,000, Abcam, #ab62341). On the second day, sections were rinsed with 1× TBS and then incubated in 0.3% H_2O_2 in TBS for 30 min. After several rinses, sections were incubated in the following secondaries for 2 h: biotinylated donkey-anti-rabbit (1:250, Jackson ImmunoResearch Laboratories, #711-065-152) and AlexaFluor488 donkey-anti-chicken (1:250, Jackson ImmunoResearch Laboratories, #703-545-155). After several rinses, sections were incubated in ABC Elite in 1× TBS (20ul of each A and B, VectorLabs, # PK-6100) for 1 h. After several rinses, as much TBS was removed from the sections as possible and 50 µl of CY3 TSA (1:100 in supplied buffer, PerkinElmer, #SAT704A001EA) was applied to each slide with a coverslip to ensure distribution across all the tissue for 5 min. After TSA, sections were thoroughly rinsed with 1× TBS and visualized wet on an epifluroescent microscope to ensure the TSA reaction worked. Sections were then incubated overnight in rabbit anti-cleaved caspase-3 (Asp175) (1:100, Cell Signaling Technologies, #9661) in blocking solution. After several rinses, sections were incubated in CY5 donkey anti-rabbit secondary for 2 h (1:250, Jackson ImmunoResearch Laboratories, catalog #711-175-152). Sections were then rinsed, counterstained with DAPI, allowed to air dry and coverslipped with DPX mounting media (Sigma, Aldrich, catalog #06522). Sections were visualized and imaged with a Zeiss LSM700 confocal microscope.

Imaging and analysis. For analysis of VGLUT puncta levels, images were acquired on a confocal LSM 710 (Zeiss) at 100× magnification (Plan-Apochromat 100×/1.46 Oil DIC M27) and zoom of 2.5 (pixel size 0.033 µm in the x-y plane). Analysis of VGLUT puncta consisted of post-processing in ImageJ using the 'find maxima' function to determine puncta number. Colocalization masks were generated in Zeiss imaging software ZEN using the colocalization function. Thresholding was performed to remove any negative 'black' space. Any adjustments in brightness and contrast were employed across the entire image. The analysis was done blind to experimental conditions.

Spine analysis was performed as previously described[23]. Dendritic segments 50–150 µm away from the soma were randomly chosen from AAV infected cells that express GFP. Images were acquired on a confocal LSM 710 (Zeiss) for morphological analysis as described previously, using a 100x objective and an xyz voxel size of 0.03 × 0.03 × 0.1 µm. Dendrites were selected from the medial shell aspect of vSTR. An average of 10 dendrites per animal totaling approximately 1,000 dendritic spines per experimental group were analyzed. For quantitative analysis of spine size, shape and volume, NeuronStudio was employed using the rayburst algorithm previously described[24]. The analysis was done blind to experimental conditions.

For representative sagittal slices demonstrating area of infection a LSM 780 (Zeiss) was employed. Images were acquired at 10× (EC Plan-Neofluar 10×/0.30 M27) using the tile scan function. Insets were acquired at 10× with the same objective.

Statistics. All data are expressed as the mean ± s.e.m. excluding SI ratio and stubby spine densities, which are shown as a scatterplot with the mean. Mean differences between groups were determined using either a one- or two-way analysis of variance (ANOVA) followed by Newman Keuls *post hoc* tests when the main effect was significant at $P < 0.05$. Mean differences in dendritic spine density and social interaction ratio were analyzed using unpaired two-sided *t* tests. Statistical analyses were performed using Prism 6.0 (GraphPad Software). All data were tested and shown to exhibit normality and equal variances. No statistical methods were used to predetermine sample sizes but our sample sizes are similar to those reported in previous publications[4].

A **Supplementary Methods Checklist** is available.

21. Burger, C. *et al. Mol. Ther.* **10**, 302–317 (2004).
22. Sparta, D.R. *et al. Nat. Protoc.* **7**, 12–23 (2012).
23. Radley, J.J. *et al. Cereb. Cortex* **16**, 313–320 (2006).
24. Rodriguez, A., Ehlenberger, D.B., Dickstein, D.L., Hof, P.R. & Wearne, S.L. *PLoS One* **3**, e1997 (2008).

doi:10.1038/nn.4034